PHILOSOPHICAL TRANSACTIONS A

rsta.royalsocietypublishing.org

Research

**Cite this article:** Bak MS, Cappelli MA. 2015 Numerical studies of nitric oxide formation in nanosecond-pulsed discharge-stabilized flames of premixed methane/air. *Phil. Trans. R. Soc. A* **373**: 20140331.
http://dx.doi.org/10.1098/rsta.2014.0331

Accepted: 26 May 2015

One contribution of 14 to a theme issue 'Physics and chemistry of plasma-assisted combustion'.

**Subject Areas:**
plasma physics, energy

**Keywords:**
plasma-assisted combustion, nitric oxide, nanosecond-pulsed discharge

**Author for correspondence:**
Moon Soo Bak
e-mail: moonsoo@skku.edu

# Numerical studies of nitric oxide formation in nanosecond-pulsed discharge-stabilized flames of premixed methane/air

Moon Soo Bak[1,2] and Mark A. Cappelli[2]

[1]School of Mechanical Engineering, Sungkyunkwan University, Chun-chun-dong 300, Jangan-gu, Suwon, Gyunggi-do 440-746, South Korea
[2]Department of Mechanical Engineering, Stanford University, Stanford, CA 94305–3032, USA

A simulation is developed to investigate the kinetics of nitric oxide (NO) formation in premixed methane/air combustion stabilized by nanosecond-pulsed discharges. The simulation consists of two connected parts. The first part calculates the kinetics within the discharge while considering both plasma/combustion reactions and species diffusion, advection and thermal conduction to the surrounding flow. The second part calculates the kinetics of the overall flow after mixing the discharge flow with the surrounding flow to account for the effect that the discharge has on the overall kinetics. The simulation reveals that the discharge produces a significant amount of atomic oxygen (O) as a result of the high discharge temperature and dissociative quenching of excited state nitrogen by molecular oxygen. This atomic oxygen subsequently produces hydroxyl (OH) radicals. The fractions of these O and OH then undergo Zel'dovich reactions and are found to contribute to as much as 73% of the total NO that is produced. The post-discharge simulation shows that the NO survives within the flow once produced.

## 1. Introduction

Combustion has been the dominant energy resource for electricity generation and propulsion. However, as regulations on the emission of carbon dioxide and other pollutants become stricter, combustion will be

THE ROYAL SOCIETY PUBLISHING

forced to move towards operation under fuel-lean conditions. While the relatively low-flame temperature associated with fuel-lean combustion suppresses the formation of nitric oxide (NO) and soot, the flame is rather unstable because of its lower intrinsic laminar flame speed. Many studies have been carried out on methods of stabilizing fuel-lean combustion. Conventional methods have used bluff bodies [1] and tangential flows [2], creating stagnant flows that provide a longer flow residence time. Recently, non-equilibrium plasmas have been used for flame holding [3]. Among these non-equilibrium plasma sources, nanosecond-pulsed repetitive discharges have been used because of their effectiveness in creating high-density plasmas with a lower required power budget when compared with other types of plasmas [4]. Studies have shown that these discharges are effective in shortening ignition delay times [5,6] and in flame holding [7–9]. This enhanced flame stability has been attributed to the production of radicals such as atomic oxygen (O) in significant amounts within the plasma [10–12].

Although the reactive species that are formed in the plasma seem to contribute to flame stabilization, it is expected that these species can also participate in forming NO. Recent experimental studies [13–15] have reported that the level of NO that is formed in the plasma can be higher than that associated with the combustion process itself. They suggested that this is because molecular oxygen dissociates into atomic oxygen within the plasma and that these O radicals subsequently participate in NO formation through the Zel'dovich mechanism [16], described by the following two reactions:

$$\left.\begin{aligned} N_2 + O &\Leftrightarrow NO + N \\ \text{and} \quad N + O_2 &\Leftrightarrow NO + O. \end{aligned}\right\} \tag{1.1}$$

The reaction of atomic nitrogen with the hydroxyl radical

$$N + OH \Leftrightarrow NO + H \tag{1.2}$$

is also known to contribute significantly to the overall NO formation and the three above reactions are often referred to as the extended Zel'dovich mechanism.

While this reaction pathway for NO seems to be likely, we note that few studies have carried out detailed kinetic simulations of NO formation in plasma-assisted combustion configurations. As described here, we have carried out these kinetic simulations to quantify the relative contributions of plasma and combustion reactions to NO formation.

## 2. Simulations

A schematic of the simulated configuration is shown in figure 1. We simulate conditions similar to that reported in a previous experimental study [15]. The pressure and temperature are 1 atm and 300 K, respectively, and methane is premixed with air at an equivalence ratio of $\phi = 0.55$. Combustion is assumed to occur in a confined cylindrical channel (8 cm inner diameter), and the premixed inlet flow speed is 27.6 cm $s^{-1}$ (e.g. a volume flow rate of 5 $m^3$ $h^{-1}$). High-voltage pulses (5.3 kV peak voltage and 10 ns pulse width with a 3 ns rise-time and 4 ns fall-time) are applied at a frequency of 30 kHz between electrodes. The electrodes are horizontally oriented and vertically separated by 4 mm to form a vertically oriented discharge plasma (shown as the small vertical cylinder in figure 1). The discharge plasma tends to be filamentary under these conditions, and the diameter of the filamentary discharge is taken to be 400 μm, similar to the size of the luminous regions seen in the experiments.

The computation is conducted in two parts. In the first part of the simulation, the kinetics of the discharge is calculated for both constant volume and constant pressure conditions, considering species diffusion, advection and thermal conduction, which are all necessary because of its relatively small size. The discharge kinetics is expected to be bounded by that calculated assuming a constant volume (appropriate for times less than the gas dynamic expansion time), and that calculated assuming constant pressure (appropriate for longer times, as the discharge region expands as a result of the increased temperature). The discharge is treated as a control volume

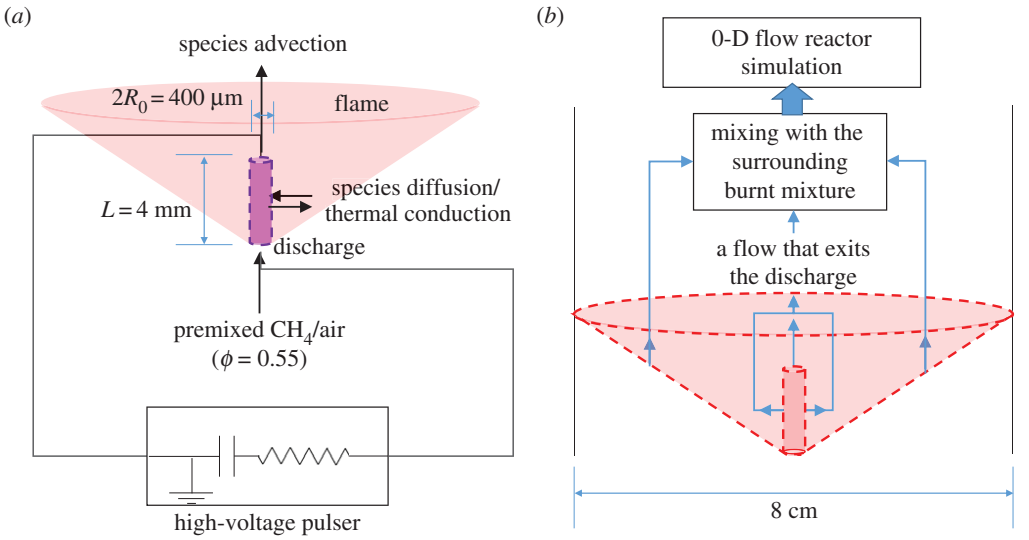


**Figure 1.** The schematic for a two-step kinetic simulation of discharge-stabilized combustion of premixed methane/air. (*a*) Discharge kinetic simulation and (*b*) post-discharge simulation. (Online version in colour.)

with a cylindrical shape and its state is assumed to be spatially uniform. The diffusion and conduction processes occur with the surroundings through the side boundary, and advection occurs through the lower and upper boundary. We treat the surrounding flow to be completely combusted since the time between discharge pulses at this repetition rate is much shorter than the time which characterizes species diffusion and advection. The composition of this burnt co-flow is calculated prior to the simulation by letting the unburnt mixture react at an adiabatic flame temperature of 1574 K under conditions of constant pressure and temperature. Fresh unburnt gases from the inlet flow enter the discharge region through the lower boundary, and the burnt mixture exits through the upper boundary. In addition to the species kinetics, the species fluxes are also calculated to study the effect of the flow that exits the discharge region on the kinetics of the surrounding flow in the second part of the simulation. The second part of the simulation mixes the discharge flow with the bypassed surrounding flow. The mixing is assumed to occur instantaneously in time and the final mixture is assumed to be homogeneous. The computation is carried out in zero-dimensions and advanced until the species densities and temperature reach their steady-state values.

The discharge simulation (assuming constant volume) solves the following energy and species conservation equations:

$$\frac{\mathrm{d}T}{\mathrm{d}t} = \frac{1}{\sum_{\mathrm{species},j} c_{\mathrm{v},j} n_j} \left[ e n_{\mathrm{e}} \mu_{\mathrm{e}} E^2 + \sum_{\mathrm{species},j} \left( \begin{array}{c} -h_{\mathrm{f},j}\dot{\omega}_{1,j} - u_{\mathrm{s},j}\frac{\mathrm{d}n_j}{\mathrm{d}t} - D_j h^{\dagger}_{\mathrm{s},j} \frac{n_{\mathrm{total}}+n_{\mathrm{total,coflow}}}{2} \frac{c_j - c_{j,\mathrm{coflow}}}{R^2} \\ -V_{\mathrm{c}} \frac{h^*_{\mathrm{s},j} n^*_j}{R/2} + V_{\mathrm{adv}} \frac{h_{\mathrm{s},j,\mathrm{initial}} n_{j,\mathrm{initial}}}{L} - V^*_{\mathrm{adv}} \frac{h_{\mathrm{s},j} n_j}{L} \\ -k \frac{T - T_{\mathrm{coflow}}}{R^2} \end{array} \right) \right] \tag{2.1}$$

and

$$\frac{\mathrm{d}n_j}{\mathrm{d}t} = \dot{\omega}_{1,j} - D_j \frac{n_{\mathrm{total}} + n_{\mathrm{total,coflow}}}{2} \frac{c_j - c_{j,\mathrm{coflow}}}{R^2} - V_{\mathrm{c}} \frac{n^*_j}{R/2} + V_{\mathrm{adv}} \frac{n_{j,\mathrm{initial}}}{L} - V^*_{\mathrm{adv}} \frac{n_j}{L}, \tag{2.2}$$

where

$$\dot{\omega}_{1,j} = \sum_{\mathrm{reactions}} (\nu'_j - \nu_j) \left[ k_{\mathrm{f}} \prod_i n^{\nu_i}_{\mathrm{reac},i} - k_{\mathrm{b}} \prod_i n^{\nu'_i}_{\mathrm{prod},i} \right] \tag{2.3}$$

for the reaction,

$$\sum_i \nu_i n_{\mathrm{reac},i} \underset{k_\mathrm{b}}{\overset{k_\mathrm{f}}{\rightleftharpoons}} \sum_i \nu_i' n_{\mathrm{prod},i}. \tag{2.4}$$

By contrast, the constant pressure simulation solves the energy and species concentration equations given as

$$\frac{\mathrm{d}T}{\mathrm{d}t} = \frac{1}{\sum_{\mathrm{species},j} c_{\mathrm{p},j} n_j} \left[ e n_\mathrm{e} \mu_\mathrm{e} E^2 \quad + \sum_{\mathrm{species},j} \left( \begin{array}{c} -h_{\mathrm{f},j}\dot{\omega}_{1,j} - h_{\mathrm{s},j}\dot{\omega}_{2,j} - D_j h^\dagger_{\mathrm{s},j} \frac{n_\mathrm{total}+n_{\mathrm{total,coflow}}}{2} \frac{c_j - c_{j,\mathrm{coflow}}}{R^2} \\ -V_\mathrm{c} \frac{h^*_{\mathrm{s},j} n^*_j}{R/2} + V_\mathrm{adv} \frac{h_{\mathrm{s},j,\mathrm{initial}} n_{j,\mathrm{initial}}}{L} - V^*_\mathrm{adv} \frac{h_{\mathrm{s},j} n_j}{L} \\ -k \frac{T - T_\mathrm{coflow}}{R^2} \end{array} \right) \right] \tag{2.5}$$

and

$$\frac{\mathrm{d}n_j}{\mathrm{d}t} = \dot{\omega}_{2,j} - n_j \left( \frac{\sum_{\mathrm{species},i} \dot{\omega}_{2,i}}{\sum_{\mathrm{species},i} n_i} + \frac{1}{T} \frac{\mathrm{d}T}{\mathrm{d}t} \right), \tag{2.6}$$

where

$$\dot{\omega}_{2,j} = \dot{\omega}_{1,j} - D_j \frac{n_\mathrm{total} + n_{\mathrm{total,coflow}}}{2} \frac{c_j - c_{j,\mathrm{coflow}}}{R^2} - V_\mathrm{c} \frac{n^*_j}{R/2} + V_\mathrm{adv} \frac{n_{j,\mathrm{initial}}}{L} - V^*_\mathrm{adv} \frac{n_j}{L}. \tag{2.7}$$

Since the discharge volume changes under conditions of constant pressure, the temporal change of discharge radius is described by

$$\frac{\mathrm{d}R}{\mathrm{d}t} = R \sqrt{\frac{\sum_{\mathrm{species},i} \dot{\omega}_{2,i}}{\sum_{\mathrm{species},i} n_i} + \frac{1}{T} \frac{\mathrm{d}T}{\mathrm{d}t}} \quad \text{and} \quad R(t=0) = R_0. \tag{2.8}$$

We assume that the discharge length is constant. In equations (2.1)–(2.8), $n_j$ and $c_j$ are the number density and mole fraction of species $j$, $n_\mathrm{total}$ is the total number density, $\nu_j$, $c_{\mathrm{v},j}$, $c_{\mathrm{p},j}$, $h_{\mathrm{f},j}$, $u_{\mathrm{s},j}$ and $h_{\mathrm{s},j}$ are the corresponding stoichiometric coefficients, heat capacity at constant volume, heat capacity at constant pressure, and formation enthalpy, and sensible internal energy and enthalpy. We note that we take $h^\dagger_{\mathrm{s},j} = h_{\mathrm{s},j}$ if $c_j - c_{j,\mathrm{coflow}} > 0$ otherwise $h^\dagger_{\mathrm{s},j} = h_{\mathrm{s},j,\mathrm{coflow}}$, and $n^*_j = n_j$ and $h^*_{\mathrm{s},j} = h_{\mathrm{s},j}$ if $V_\mathrm{c} > 0$ otherwise $n^*_j = n_{j,\mathrm{coflow}}$ and $h^*_{\mathrm{s},j} = h_{\mathrm{s},j,\mathrm{coflow}}$. $k_\mathrm{f}$ and $k_\mathrm{b}$ are the forward and reverse reaction rate coefficients, $E$ is the electric field, $T_\mathrm{e}$ is the electron temperature, $T$ is the gas temperature, $\mu_\mathrm{e}$ is electron mobility, $D_\mathrm{j}$ is the diffusion coefficient of species $j$, $k$ is the thermal conductivity, and $R$ and $L$ are the effective lengths for diffusion (i.e. 200 µm) and advection (i.e. 4 mm), respectively. Finally, $V_\mathrm{c}$ and $V^*_\mathrm{adv}$ are the local convection and advection velocities, calculated to satisfy

$$V_\mathrm{c} = \frac{\sum_{\mathrm{species},j} -D_j M_j ((n_\mathrm{total} + n_{\mathrm{total,coflow}})/2)((c_j - c_{j,\mathrm{coflow}})/2R)}{\sum_{\mathrm{species},j} M_j n^*_j} \tag{2.9}$$

and

$$V^*_\mathrm{adv} = \frac{\rho_\mathrm{initial} \pi R_0^2}{\rho \pi R^2} V_\mathrm{adv}. \tag{2.10}$$

Here $\rho$ is the gas density. In the simulation, the pulse generating circuit (a charging/discharging capacitor) is also considered when calculating the net electric field. We assume that a capacitor stores an energy $W = 1$ mJ and delivers a high voltage to the electrodes. As the current flows into the capacitor, the charges accumulate and determine the net applied voltage. The equations for

the net voltage ($V$) and electric field ($E$) are

$$V = V_{\mathrm{p}} - \frac{Q}{C_{\mathrm{pulser}}} - en_{\mathrm{e}}\mu_{\mathrm{e}}E\pi R^2 Z \tag{2.11}$$

and

$$E = \frac{V}{L}. \tag{2.12}$$

Here $V_{\mathrm{p}}$ is the programmed applied voltage, $e$ is the electron charge and $Z$ is the pulse generator output impedance, which is assumed to be 100 $\Omega$. The charge accumulation ($Q$) and the time-varying capacitance ($C_{\mathrm{pulser}}$) are expressed as

$$Q(t) = \int_0^t en_{\mathrm{e}}\mu_{\mathrm{e}}E\pi R^2 \mathrm{d}t' \tag{2.13}$$

and

$$C_{\mathrm{pulser}}(t) = \frac{2W}{V_{\mathrm{p}}(t)^2}. \tag{2.14}$$

In addition to the computation of species densities and gas temperature, the species flux that exits the discharge volume is also calculated to allow us to investigate their effect on the kinetics of its surrounding flow.

The kinetic simulation for the post-discharge region solves the energy and species concentration equations

$$\sum_{\mathrm{species},j} \frac{\mathrm{d}(n_j \int_{298.15K}^{T} c_{\mathrm{p},j}\mathrm{d}T')}{\mathrm{d}t} = -\sum_{\mathrm{species},j} h_{\mathrm{f},j}\dot{\omega}_j \tag{2.15}$$

and

$$\frac{\mathrm{d}n_j}{\mathrm{d}t} = \dot{\omega}_j - n_j\left(\frac{\sum_{\mathrm{species},i}\dot{\omega}_i}{\sum_{\mathrm{species},i} n_i} + \frac{1}{T}\frac{\mathrm{d}T}{\mathrm{d}t}\right) \tag{2.16}$$

where

$$\dot{\omega}_j = \sum_{\mathrm{reactions}} (\nu_j' - \nu_j)\left[k_{\mathrm{f}}\prod_i n_{\mathrm{reac},i}^{\nu_i} - k_{\mathrm{b}}\prod_i n_{\mathrm{prod},i}^{\nu_i'}\right]. \tag{2.17}$$

By assuming that the two streams are perfectly mixed, a zero-dimensional simulation can be carried out and since the mixing is taking place downstream of the plasma, we neglect plasma heating, diffusion and advection processes.

Detailed kinetics for both plasma and combustion reactions are included in the simulation. GRI-Mech v. 3.0 [17] is used for premixed methane/air combustion. The plasma kinetic mechanism used in this study is systematically reduced from the one proposed by Kossyi *et al.* [18] for dry air and contains electron-impact excitation, dissociation, ionization of $N_2$ and $O_2$, ion conversion, electron–ion recombination, quenching of excited states of $N_2$ ($N_2^*$) by $N_2$ and $O_2$, and other reactions between neutral species [19]. Since the discharge is in a combustible mixture, it will contain $CH_4$, $CO_2$ and $H_2O$ as major components, and we include electron-impact dissociation, ionization of $CH_4$, $CO_2$ and $H_2O$, electron–ion recombination, and quenching of $N_2^*$ by $CH_4$ and $H_2O$. The complete plasma reaction mechanism is presented in table 1. The electron-impact cross sections for $N_2$ [20], N [21], $O_2$, $CO_2$ [22], O, $H_2O$ [23] and $CH_4$ [24] are taken from databases compiled from different sources. All rate coefficients except the electron-impact reactions are adopted from the previous literature [9,17,18,25–29], whereas the rate coefficients of the electron-impact reactions, electron mobility and electron temperature are calculated as a function of the reduced electric field ($E/n$) using the Bolsig+ software package [30].

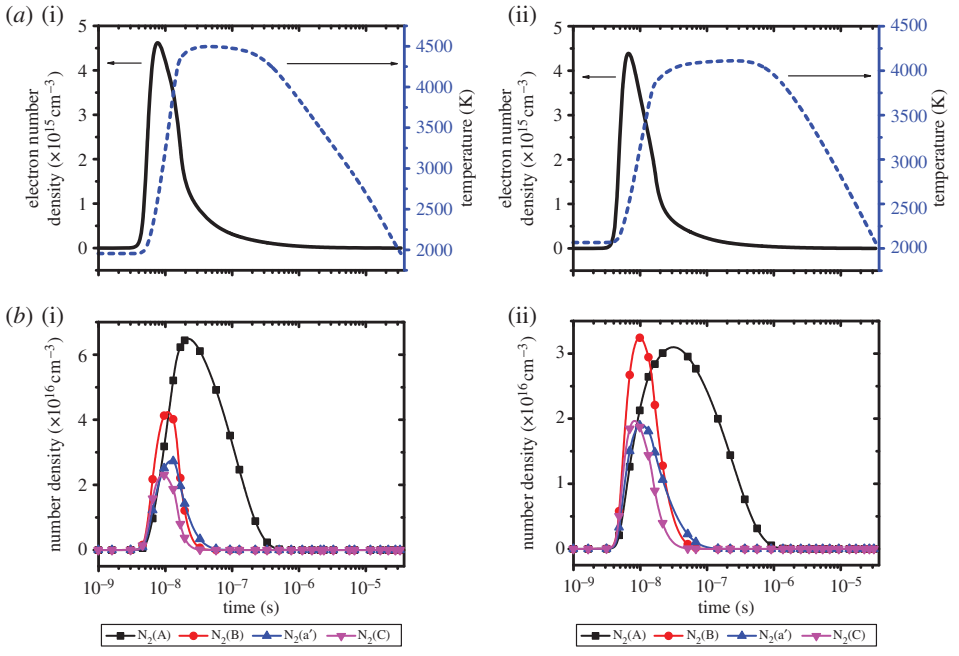


**Figure 2.** (*a*) Time evolution of electron density, gas temperature and (*b*) densities of excited states of nitrogen ($N_2^*$) within the discharge during a single period, calculated under (*a*(i),*b*(i)) constant volume and (*a*(ii),*b*(ii)) constant pressure conditions. (Online version in colour.)

Thermodynamic properties of species (e.g. heat capacity and enthalpies) are calculated using the NASA polynomials complied by Burcat [31] instead of those included in the GRI-MECH v. 3.0 because of a required range of discharge temperature.

# 3. Results

## (a) Results of discharge kinetic simulations

The computation is carried out for tens of discharge pulses to quasi-steady state for initial species densities and gas temperature. The time evolution of the electron density, gas temperature and electronically excited nitrogen (e.g. $N_2^*$) densities within the discharge during a single discharge period are shown in figure 2 for both constant volume and constant pressure conditions. Under conditions of constant volume, the electron density and gas temperature peak at $4.6 \times 10^{15}$ cm$^{-3}$ and 4500 K, respectively. $N_2^*$ is also substantially produced because of the high electron density, reaching a peak number density of $1.38 \times 10^{17}$ cm$^{-3}$. The high electron and excited state densities and gas temperature are common for this type of discharge plasma, and similar levels had been reported from previous simulations and experimental studies [32]. The populations of electrons and $N_2^*$ are quenched immediately following the voltage pulse. The electron quenching is mainly due to electron–ion recombination and the quenching of $N_2^*$ is mainly due to collisions with neutral species. Similar trends for the electron and $N_2^*$ densities, and temperature, are obtained for constant pressure conditions. However, the $N_2^*$ densities are found to be lower for times more than 30 ns and the peak temperature is decreased by 400 K because of volume expansion of the discharge.

The time evolution of the number densities of major combustion species ($CH_4$, $O_2$, $CO_2$ and $H_2O$) and of minor combustion species (CO, O, OH, N and NO) within the discharge during a single discharge period are shown in figure 3. Under conditions of constant pressure, all of

**Table 1.** Plasma reactions used for the plasma-assisted combustion simulation.

| | reaction | refs | | reaction | refs |
|---|---|---|---|---|---|
| R1 | $N_2+e\rightarrow N_2(A)+e$ | [20] | R41 | $e+CO_2^+ +M\rightarrow CO_2+M$ | [a] |
| R2 | $N_2+e\rightarrow N_2(B)+e$ | [20] | R42 | $e+H_2O^+ +M\rightarrow H_2O+M$ | [a] |
| R3 | $N_2+e\rightarrow N_2(a')+e$ | [20] | R43 | $O^- +O\rightarrow O_2+e$ | [18] |
| R4 | $N_2+e\rightarrow N_2(C)+e$ | [20] | R44 | $N_2(A)+O_2\rightarrow N_2+O_2$ | [18] |
| R5 | $N+e\rightarrow N(^2D)+e$ | [21] | R45 | $N_2(A)+O_2\rightarrow N_2+2O$ | [18] |
| R6 | $N+e\rightarrow N(^2P)+e$ | [21] | R46 | $N_2(A)+CH_4\rightarrow N_2+CH_3+H$ | [25] |
| R7 | $O_2+e\rightarrow 2O+e$ | [22] | R47 | $N_2(A)+N\rightarrow N_2+N(^2P)$ | [18] |
| R8 | $O_2+e\rightarrow O+O(^1D)+e$ | [22] | R48 | $N_2(A)+O\rightarrow NO+N(^2D)$ | [18] |
| R9 | $O_2+e\rightarrow O+O(^1S)+e$ | [22] | R49 | $N_2(A)+O\rightarrow N_2+O(^1S)$ | [18] |
| R10 | $O+e\rightarrow O(^1D)+e$ | [23] | R50 | $N_2(A)+NO\rightarrow N_2+NO$ | [18] |
| R11 | $O+e\rightarrow O(^1S)+e$ | [23] | R51 | $N_2(B)+N_2\rightarrow N_2(A)+N_2$ | [18] |
| R12 | $CH_4+e\rightarrow CH_3+H+e$ | [24] | R52 | $N_2(B)+O_2\rightarrow N_2+2O$ | [18] |
| R13 | $CO_2+e\rightarrow CO+O+e$ | [22] | R53 | $N_2(B)+CH_4\rightarrow N_2+CH_3+H$ | [26] |
| R14 | $H_2O+e\rightarrow OH+H+e$ | [23] | R54 | $N_2(B)+CO_2\rightarrow N_2+CO_2$ | [26] |
| R15 | $H_2O+e\rightarrow O(^1S)+H_2+e$ | [23] | R55 | $N_2(B)+H_2O\rightarrow N_2+OH+H$ | [b] |
| R16 | $N_2+e\rightarrow N_2^+ +2e$ | [20] | R56 | $N_2(a')+N_2\rightarrow N_2(B)+N_2$ | [18] |
| R17 | $O_2+e\rightarrow O_2^+ +2e$ | [22] | R57 | $N_2(a')+O_2\rightarrow N_2+2O$ | [18] |
| R18 | $O_2+e\rightarrow O^- +O$ | [22] | R58 | $N_2(a')+CH_4\rightarrow N_2+CH_3+H$ | [27] |
| R19 | $CH_4+e\rightarrow CH_4^+ +2e$ | [24] | R59 | $N_2(a')+CO_2\rightarrow N_2+CO+O$ | [27] |
| R20 | $CO_2+e\rightarrow CO_2^+ +2e$ | [22] | R60 | $N_2(a')+H_2O\rightarrow N_2+OH+H$ | [28] |
| R21 | $H_2O+e\rightarrow H_2O^+ +2e$ | [23] | R61 | $N_2(a')+NO\rightarrow N_2+N+O$ | [18] |
| R22 | $N_2(A)+N_2(a')\rightarrow N_4^+ +e$ | [18] | R62 | $N_2(C)\rightarrow N_2(B)+h\nu$ | [18] |
| R23 | $N_2(a')+N_2(a')\rightarrow N_4^+ +e$ | [18] | R63 | $N_2(C)+N_2\rightarrow N_2(a')+N_2$ | [18] |
| R24 | $N_2^+ +e\rightarrow 2N$ | [18] | R64 | $N_2(C)+O_2\rightarrow N_2+2O$ | [18] |
| R25 | $N_2^+ +e\rightarrow N+N(^2D)$ | [18] | R65 | $N_2(C)+CH_4\rightarrow N_2+CH_3+H$ | [29] |
| R26 | $O_2^+ +e\rightarrow 2O$ | [18] | R66 | $N_2(C)+CO_2\rightarrow N_2+CO+O$ | [29] |
| R27 | $N_4^+ +e\rightarrow 2N_2$ | [18] | R67 | $N_2(C)+H_2O\rightarrow N_2+OH+H$ | [29] |
| R28 | $CH_4^+ +e\rightarrow CH_3+H$ | [9] | R68 | $N(^2D)+O_2\rightarrow NO+O$ | [18] |
| R29 | $CO_2^+ +e\rightarrow CO+O$ | [9] | R69 | $N(^2D)+O_2\rightarrow NO+O(^1D)$ | [18] |
| R30 | $H_2O^+ +e\rightarrow O+2H$ | [9] | R70 | $N(^2P)+O_2\rightarrow NO+O$ | [18] |
| R31 | $NO^+ +e\rightarrow N(^2D)+O$ | [18] | R71 | $O(^1D)+N_2\rightarrow O+N_2$ | [18] |
| R32 | $N_3^+ +e\rightarrow N_2+N$ | [18] | R72 | $O(^1D)+O_2\rightarrow O+O_2$ | [18] |
| R33 | $e+e+N_2^+\rightarrow e+N_2$ | [18] | R73 | $O(^1D)+NO\rightarrow N+O_2$ | [18] |
| R34 | $e+e+O_2^+\rightarrow e+O_2$ | [18] | R74 | $O(^1S)+O\rightarrow O(^1D)+O$ | [18] |
| R35 | $e+e+CH_4^+\rightarrow e+CH_4$ | [a] | R75 | $N_2^+ +2N_2\rightarrow N_4^+ +N_2$ | [18] |
| R36 | $e+e+CO_2^+\rightarrow e+CO_2$ | [a] | R76 | $N_2^+ +N_2(A)\rightarrow N_3^+ +N$ | [18] |
| R37 | $e+e+H_2O^+\rightarrow e+H_2O$ | [a] | R77 | $O_2^+ +N\rightarrow NO^+ +O$ | [18] |
| R38 | $e+N_2^+ +M\rightarrow N_2+M$ | [18] | R78 | $O_2^+ +NO\rightarrow NO^+ +O_2$ | [18] |
| R39 | $e+O_2^+ +M\rightarrow O_2+M$ | [18] | R79 | $N_4^+ +N_2\rightarrow N_2^+ +2N_2$ | [18][c] |
| R40 | $e+CH_4^+ +M\rightarrow CH_4+M$ | [a] | R80 | $N_4^+ +O_2\rightarrow O_2^+ +2N_2$ | [18] |

[a]This rate coefficient is assumed to be same as those of other ions of $N_2^+$ and $O_2^+$ [18].

[b]This rate coefficient is assumed based on [26].

[c]This rate coefficient is assumed not to exceed $2.5\times10^{10}$ cm$^{-3}$.

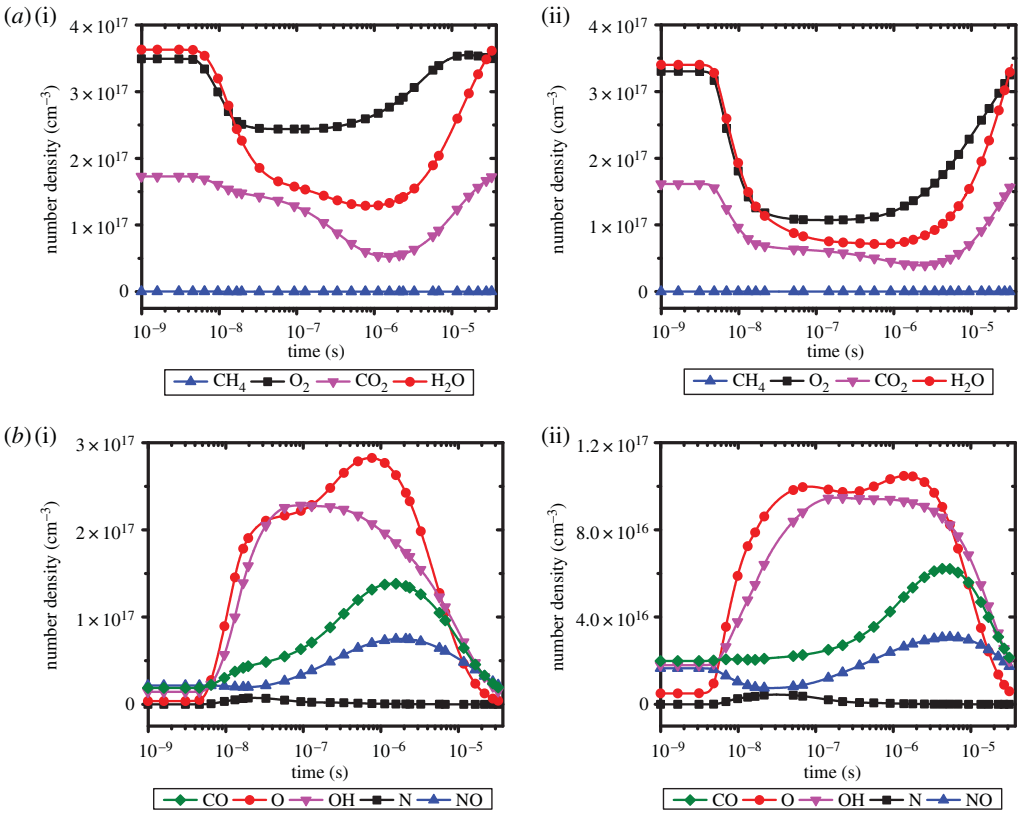


**Figure 3.** (*a*) Time evolution of major combustion species ($CH_4$, $O_2$, $CO_2$ and $H_2O$) and (*b*) minor combustion species densities (CO, O, OH, N and NO) within the discharge during a single period, calculated under (*a*(i),*b*(i)) constant volume and (*a*(ii),*b*(ii)) constant pressure conditions. (Online version in colour.)

the species densities are decreased substantially as a result of discharge volume expansion. The kinetics is also slower compared with that of constant volume. Based on the constant pressure results, the concentration of methane remains relatively low as the timescale for the species advection is not short enough to refresh the discharge region with the unburnt mixture. Among the minor species, atomic oxygen (O) and hydroxyl (OH) radicals are produced in significant amounts. Their densities are found to reach $1.1 \times 10^{17}\,\mathrm{cm}^{-3}$ and $9.5 \times 10^{16}\,\mathrm{cm}^{-3}$, respectively. A reaction path analysis revealed that there is a rapid production of O through dissociative quenching of $N_2^*$ with $O_2$, but the thermal decomposition of $H_2O$ and $CO_2$ as a result of the high discharge temperature plays an important role in determining the peak levels of O and OH densities under the studied conditions. The produced O and OH radicals then undergo either recombination to form $CO_2$ and $H_2O$ as the gas temperature decreases after the pulse or the extended Zel'dovich NO-forming reactions (see equations (1.1) and (1.2)). The level of nitric oxide (NO) is found to be high because of the high O and OH densities and temperature. Its peak density reaches $3.1 \times 10^{16}\,\mathrm{cm}^{-3}$. It is found that most of the produced NO (e.g. 73%) is attributed to the Zel'dovich reactions and the quenching of $N_2$ (A) with O (e.g. 27%) contributes to a majority of the rest. The high concentrations of these minor combustion species finally decrease as a result of species diffusion and advection towards the surrounding burnt flow. Since the concentrations of NO and other reactive species such as O, OH and N remain at levels that are higher within the discharge than in the surrounding flow, the diffusion and advection of these species into the surrounding flow may be important for the accurate prediction of NO formation.

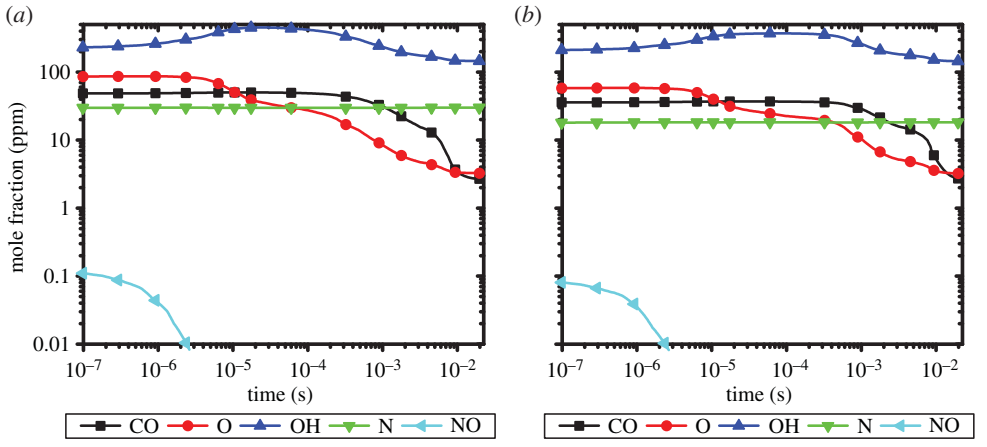


**Figure 4.** Time evolution of minor combustion species densities (CO, O, OH, N and NO) at post-discharge regions. Each result is based on the prior discharge simulation result of (*a*) constant volume and (*b*) constant pressure. (Online version in colour.)

## (b) Results of post-discharge simulations

The flux of species from the discharge surfaces is first calculated and then this flow that exits the discharge is mixed with the surrounding burnt flow. The time evolution of a selection of minor combustion species (CO, O, OH, N and NO) with discharge simulations carried out under conditions of constant volume and constant pressure are shown in figure 4. Immediately after mixing, the minor species densities are found to be higher than their steady-state values as the discharge supplies reactive species at much higher densities. The post-discharge flow reaches steady state within 10 ms with the NO density increasing only slightly during this time. This is expected since NO is hard to destroy once it is formed. The mole fraction of NO is found to be between 18 ppm (for the case of constant pressure) and 30 ppm (for the case of constant volume). This level of NO is much higher than that produced from just the combustion alone (e.g. $<1$ ppm). Although fuel-lean combustion is intended to reduce NO as it leads to a relatively low-flame temperature, it is found that the discharge can contribute in a substantial way to the production of NO. We find that the amount of NO that the discharge produces depends not only on the plasma reactions but also on the discharge temperature. Future work will study the NO formation for different discharge conditions.

# 4. Conclusion

A two-step kinetic simulation is carried out to identify reaction pathways that contribute most to NO formation in premixed fuel-lean plasma-assisted combustion. It is found that the plasma discharge produces significant amounts of atomic oxygen (O) and hydroxyl (OH) radicals. Although the dissociative quenching of electronically excited nitrogen ($N_2^*$) contributes to the rapid production of O during the voltage pulse, the thermal decomposition of $H_2O$ and $CO_2$ determines the peak levels of produced O and OH densities. These O and OH then lead to form NO mostly through the extended Zel'dovich reactions. Given the flow and discharge conditions, the level of NO produced for the use of discharge is found to be substantial. Since the NO formation is sensitive to the discharge temperature, future work will study NO reactions over a range of discharge conditions.

Authors' contributions. M.S.B. and M.A.C. have made equal contributions to the design of the experiments. M.S.B. acquired all data and carried out the analysis. Both were involved in the interpretation of data and drafting of the article.

Competing interests. The authors declare that they have no competing interests.

Funding. We received no funding for this study.

## References


1. Santosh JS, Sajjad H, Tim L. 2009 Lean blowoff of bluff body stabilized flames: scaling and dynamics. *Prog. Energ. Combust.* **35**, 98–120. (doi:10.1016/j.pecs.2008.07.003)
2. Cheng RK. 1995 Velocity and scalar characteristics of premixed turbulent flames stabilized by weak swirl. *Combust. Flame* **101**, 1–14. (doi:10.1016/0010-2180(94)00196-Y)
3. Starikovskiy A, Aleksandrov N. 2013 Plasma-assisted ignition and combustion. *Prog. Energ. Combust.* **39**, 61–110. (doi:10.1016/j.pecs.2012.05.003)
4. Kruger CH, Laux CO, Yu L, Packan DM, Pierrot L. 2002 Nonequilibrium discharges in air and nitrogen plasmas at atmospheric pressure. *Pure Appl. Chem.* **74**, 337–347. (doi:10.1351/pac200274030337)
5. Bao A, Utkin YG, Keshav S, Lou G, Adamovich IV. 2007 Ignition of ethylene/air and methane/air flows by low-temperature repetitively pulsed nanosecond discharge plasma. *IEEE Trans. Plasma Sci.* **35**, 1628–1638. (doi:10.1109/TPS.2007.910143)
6. Kosarev IN, Aleksandrov NL, Kindysheva SV, Starikovskaia SM, Starikovskii AY. 2008 Kinetics of ignition of saturated hydrocarbons by nonequilibrium plasma: $CH_4$-containing mixtures. *Combust. Flame* **154**, 569–586. (doi:10.1016/j.combustflame.2008.03.007)
7. Pilla G, Galley D, Lacoste DA, Lacas F, Veynante D, Laux CO. 2006 Stabilization of a turbulent premixed flame using a nanosecond repetitively pulsed plasma. *IEEE Trans. Plasma Sci.* **34**, 2471–2477. (doi:10.1109/TPS.2006.886081)
8. Kim W, Do H, Mungal MG, Cappelli MA. 2006 Plasma-discharge stabilization of jet diffusion flames. *IEEE Trans. Plasma Sci.* **34**, 2545–2551. (doi:10.1109/TPS.2006.886084)
9. Bak MS, Do H, Mungal MG, Cappelli MA. 2012 Plasma-assisted stabilization of laminar premixed methane/air flames around the lean flammability limit. *Combust. Flame* **159**, 3128–3137. (doi:10.1016/j.combustflame.2012.03.023)
10. Stancu GD, Kaddouri F, Lacoste DA, Laux CO. 2010 Atmospheric pressure plasma diagnostics by OES, CRDS and TALIF. *J. Phys. D: Appl. Phys.* **43**, 124 002–124 010. (doi:10.1088/0022-3727/43/12/124002)
11. Bak MS, Kim W, Cappelli MA. 2011 On the quenching of excited electronic states of molecular nitrogen in nanosecond pulsed discharges in atmospheric pressure air. *Appl. Phys. Lett.* **98**, 011502. (doi:10.1063/1.3535986)
12. Mintoussov EI, Pendleton SJ, Gerbault FG, Popov NA, Starikovskaia SM. 2011 Fast gas heating in nitrogen-oxygen discharge plasma: II. Energy exchange in the afterglow of a volume nanosecond discharge at moderate pressures. *J. Phys. D: Appl. Phys.* **44**, 285 202–285 213. (doi:10.1088/0022-3727/44/28/285202)
13. Kim W, Do H, Mungal MG, Cappelli MA. 2007 Investigation of NO production and flame structure in plasma enhanced premixed combustion. *P. Combust. Inst.* **31**, 3319–3326. (doi:10.1016/j.proci.2006.07.107)
14. Lacoste DA, Moeck JP, Paschereit CO, Laux CO. 2013 Effect of plasma discharges on nitric oxide emissions in a premixed flame. *J. Propul. Power* **29**, 748–751. (doi:10.2514/1.B34819)
15. Stancu GD, Simeni MS, Laux CO. 2013 Study of nitric oxide and carbon monoxide production in plasma assisted combustion by quantum cascade laser absorption spectroscopy. In *21st Int. Symp. Plasma Chemistry, Cairns, Australia, 4–9 August*.
16. Miller JA, Bowman CT. 1989 Mechanism and modeling of nitrogen chemistry in combustion. *Prog. Energ. Combust.* **15**, 287–338. (doi:10.1016/0360-1285(89)90017-8)
17. Smith GP *et al.* 1999 *GRI-Mech home page*. http://www.me.berkeley.edu/gri_mech/.
18. Kossyi IA, Kostinsky AY, Matveyev AA, Silakov VP. 1992 Kinetic scheme of the non-equilibrium discharge in nitrogen-oxygen mixtures. *Plasma Sources Sci. Technol.* **1**, 207–220. (doi:10.1088/0963-0252/1/3/011)
19. Bak MS, Cappelli MA. 2015 A reduced set of air plasma reactions for nanosecond pulsed plasmas. *IEEE Trans. Plasma Sci.* **43**, 995–1001. (doi:10.1109/TPS.2015.2409300)
20. SIGLO database. 2014 www.lxcat.net (accessed 17 October 2014).
21. IST-Lisbon database. 2014 www.lxcat.net (accessed 17 October 2014).
22. Phelps database. 2014 www.lxcat.net (accessed 17 October 2014).
23. Morgan database. 2014 www.lxcat.net (accessed 17 October 2014).
24. Hayashi database. 2014 www.lxcat.net (accessed 17 October 2014).

25. Golde MF, Ho GH, Tao W, Thomas JM. 1989 Collisional deactivation of nitrogen (A3.SIGMA.u+, v = 0–6) by methane, carbon tetrafluoride, hydrogen, water, chlorotrifluoromethane, and chlorodifluoromethane. *J. Phys. Chem.* **93**, 1112–1118. (doi:10.1021/j100340a018)
26. Piper LG. 1992 Energy transfer studies on $N_2(X^1\Sigma_g^+,v)$ and $N_2(B^3\Pi_g)$. *J. Chem. Phys.* **97**, 270–275. (doi:10.1063/1.463625)
27. Piper LG. 1987 Quenching rate coefficients for $N_2(a'^1\Sigma_u^-)$. *J. Chem. Phys.* **87**, 1625–1629. (doi:10.1063/1.453223)
28. Umemoto H, Oku M. 2003 Production yields of H(D) atoms in the reactions of $N_2(a'^1\Sigma_u^-)$ with $H_2O$, $D_2O$, and HOD. *Bull. Chem. Soc. Jpn.* **76**, 291–294. (doi:10.1246/bcsj.76.291)
29. Albugues F, Birot A, Blanc D, Brunet H, Galy J, Millet P, Teyssier JL. 1974 Destruction of the levels $C^3\Pi_u$ ($v' = 0. v' = 1$) of nitrogen by $O_2$, $CO_2$, $CH_4$, and $H_2O$. *J. Chem. Phys.* **61**, 2695–2699.
30. Hagelaar GJM, Pitchford LC. 2005 Solving the Boltzmann equation to obtain electron transport coefficients and rate coefficients for fluid models. *Plasma Source Sci. Technol.* **14**, 722–733. (doi:10.1088/0963-0252/14/4/011)
31. Burcat A. 2001 Third Millennium Ideal Gas and Condensed Phase Thermochemical Database for Combustion, Technion-Israel Institute of Technology, TAE 867.
32. Pai DZ, Lacoste DA, Laux CO. 2010 Nanosecond repetitively pulsed discharges in air at atmospheric pressure—the spark regime. *Plasma Sources Sci. Tech.* **19**, 065015. (doi:10.1088/0963-0252/19/6/065015)